International Journal of Scientific Research in Engineering and Management (IJSREM)
Volume: 06 Issue: 05 | May - 2022 Impact Factor: 7.185 ISSN: 2582-3930

Deep Learning Methods for Registering Images with ERC

[1,2,3]S.Rama koteswararao, research scholar, Annamalai university,

Dr.S.Palanivel, associate professor, annamalai university,

Dr.G.L.N.Murthy , associate professor,LBRCE

***Abstract*—MRI images of same subject at different times are used for image registration to diagnose the prostate cancer .It is very difficult to diagnose when the image has Endorectal coil (ERC).For this we have to use iterative methods .so we are going to use deep learning methods. In this paper for forward/backward registration we are using cyclic constraint loss. Inverse constraint loss is used for diffeomorphic registration. In addition, an adaptive anatomical constraint aiming for regularizing the registration network with the use of anatomical labels is introduced. Compared with other existing methods, our approach works more efficiently with average running time less than a second and is able to obtain more visually realistic results.**

***KEYWORDS*: ERC- Endorectalcoil, MRI-Magnetic resonance imaging**

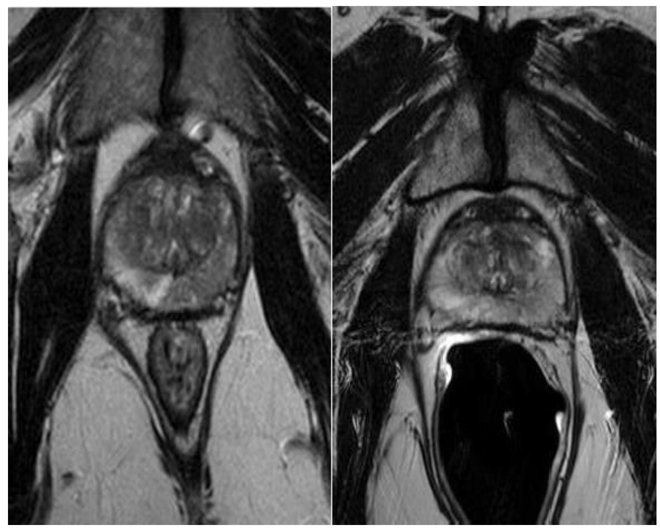

(a) Without ERC (b) With ERC

Fig. 1: MR images with/without endo-rectal coil (ERC) of the same subject showing the large prostate deformation.

I. INTRODUCTION

PROSTATE cancer is one of the most common types of cancer for men in the world. Early diagnosis of prostate cancer significantly increases the chance of survival [1]. In addition, for prostate cancer diagnosis and treatment, knowledge of the stage and grade of each lesion can help predict outcomes and facilitate appropriate treatment options. Continuous monitoring of lesions as part of active surveillance helps avoid over-treatment of prostate cancer to keep the quality of life for cancer patients. With the development of computer technology and computer graphics, medical imaging technology has made Great progress and has been widely used in clinical practice. Magnetic resonance imaging (MRI) has been commonly used in prostate cancer diagnosis and treatment [2]. For example, MRI can provide information of water molecule diffusion,blood perfusion and microcirculation status of prostate cancer. Analysis of MR images of a patient over time can help detect the change to make accurate diagnosis. However, due to the prostate deformation over the long time interval, typically one year or more, the registration of the images can be difficult. What makes it even more complicated is the change in imaging protocols between the exams. For instance, the initial MRI scans of patients may be performed with the use of endo- rectal coil (ERC) to help cancer staging. If the detected cancer is not very aggressive, the follow-up scan performed a year later will be done without ERC for the comfort of patients. As shown in Fig. 1, the large prostate appearance difference and shape deformation make the registration of MR images much more challenging. In addition, the tissues around the prostate have similar characteristic distribution with the prostate, and the presence of artifacts and fuzzy edges in the prostate region further increases the difficulty of registering prostate images..

Asterisks indicate corresponding authors. Bo Du and Jiandong Liao make equal contributions.

*B. Du and J. Liao are with School of Computer Science, institute of Artificial Intelligence, Wuhan University, Wuhan, China. (e-mail: dubo@whu.edu.cn, liaojiandong@whu.edu.cn). B. Du and J. Liao were supported in part by the National Natural Science Foundation of China under Grant 62041105 and the Science and Technology Major Project of Hubei Province under Grant 2019AEA170.

B. Turkbey is with the Molecular Imaging Program, National Cancer Institute, National Institutes of Health, Bethesda, MD 20892, USA. (e-mail: ismail.turkbey@nih.gov)

*P. Yan is with the Department of Biomedical Engineering and the Center for Biotechnology and Interdisciplinary Studies at Rensselaer Polytechnic Institute, Troy, NY 12180, USA. (e-mail: yanp2@rpi.edu).

International Journal of Scientific Research in Engineering and Management (IJSREM)
Volume: 06 Issue: 05 | May - 2022 Impact Factor: 7.185 ISSN: 2582-3930

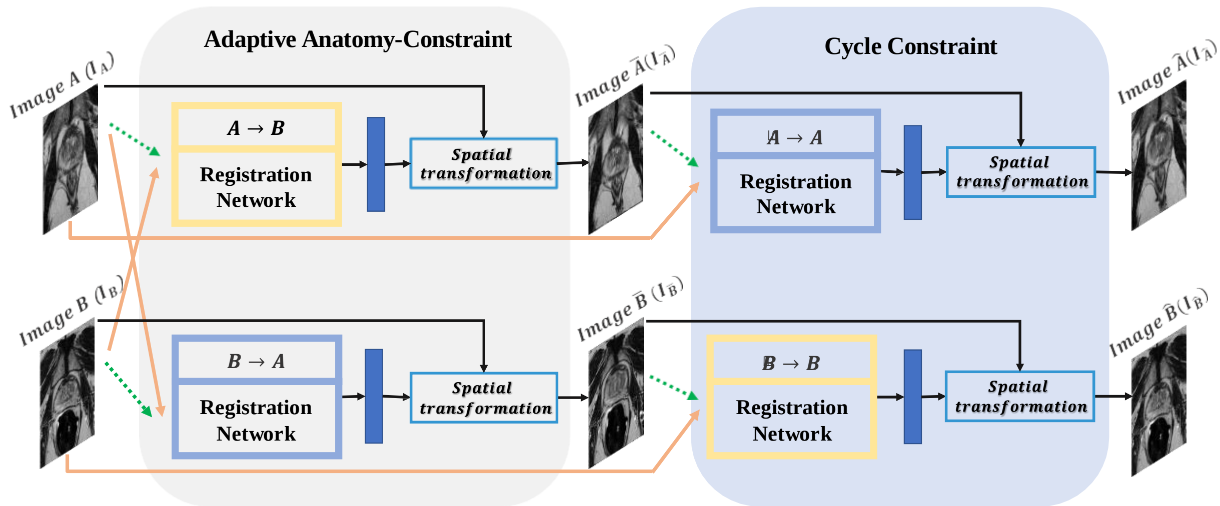

Fig. 2: Overall structure of the proposed image registration framework. Please note the difference of fixed and moving images for each registration network in those blocks, which are color coded according to the fixed image domain.

where Φ denotes the deformation field for warping the moving image M to the fixed image F. The first part $L(,)$ is used to evaluate the degree of alignment of the warped moving image ($T(M, \Phi)$) and fixed image (F). In the literature, many types of similarity metrics have been proposed for image registration. such as normalized cross correlation (NCC) [5], sum-of-squares distance (SSD) [6], mutual information (MI) [7]–[9], different similarity metrics focus on different feature information and usually choose flexibly according to the actual situation. The second part $R(\ )$ is regularization to make the generated deformation field smoother and penalizes the undesired deformation. such as topology preservation [10] and strain energy [11]. Although the classical algorithms have achieved reasonable performance, it is usually slow due to the nature of iterative optimization. In addition, it is difficult to define an appropriate similarity measure to register images.

Recently, some exciting progress has been made in applying deep learning to deformable medical image registration [12]. Those methods usually use deep learning to extract features and predict the deformation field, and finally obtain registration result through image resampling [13]. Unsupervised learning methods have been widely used in image registration, and existing deep learning-based methods are usually un super- vised [14]–[16]. For example, de Vos et al. [14] developed an end-to-end unsupervised registration method (DIRNet), whichgenerates a displacement vector field to align a pair of images. Dalca et al. [15] proposed a probabilistic generative modelby deriving an inference algorithm based on unsupervised learning. To avoid manually defining a similarity measure for loss computation, Yan et al. [17] introduced adversarial learning to multi-modality image registration. Similarly, Fan et al. [18] proposed to register images, where the registration network is trained with feedback from the discrimination network designed to judge whether a pair of registered imagesare sufficiently similar.

achieved promising results, most existing methods do not enforce inverse consistency between image pairs. That is, the registrations of $B \rightarrow A$ and $A \rightarrow B$ are two independent processes, and the inverse of $A \rightarrow B$ transformation is not equal to the transformation of $B \rightarrow A$. Such inconsistency makes the matching between image pairs poorly defined. In addition, the cycle consistency of the image is ignored in the registration process. That is to say, the registration result $\bar{A}$ can be transformed into A using the same algorithm in this paper.

To address these issues, this paper proposes a new method for registering images with large deformation. Effectiveness of the proposed method is demonstrated on registering prostate MR images of the same subject acquired at different time points with and without ERC, respectively. We propose a multi-task registration network that not only ensures the reversibility of image alignment, but also achieves symmetric registration between pairs of images. At the same time, we explore the potential links between different tasks. Inverse consistency ensures the symmetrical deformation of image pairs and cycle consistency loss overcomes the challenge of irreversible image registration. To implement these ideas, we first propose a dual-path multi-scale fusion network structure, which uses two convolutional neural networks (CNNs) to extract and fuse the features of fixed image I_f and moving image I_m respectively. Last but not least, to avoid the distraction by the potential large deformation of surrounding tissues, we design an adaptive anatomical constraint to enforce the networks to pay more attention to the prostate itself by utilizing the segmentation labels.

The remainder of the paper is organized as follows. Section II presents the proposed multi-task learning based registration in detail.

International Journal of Scientific Research in Engineering and Management (IJSREM)
Volume: 06 Issue: 05 | May - 2022 Impact Factor: 7.185 ISSN: 2582-3930

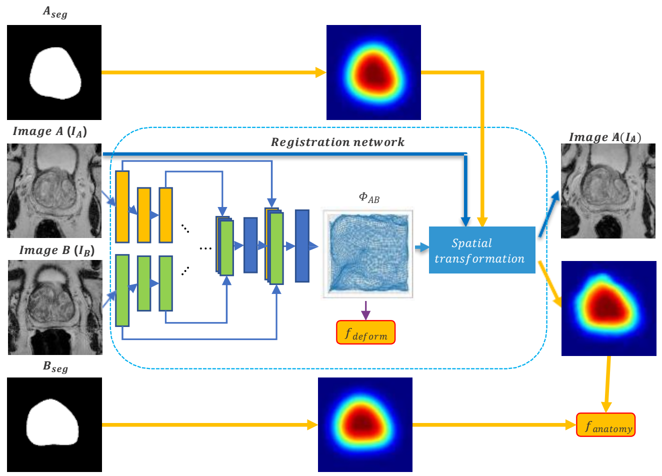

Fig. 3: Structure of the proposed adaptive anatomy-constrained image registration network. Take image A as the moving image and image B as the fixed image as an example.

II. Multi-task learning based Registration

In this paper, we propose to exploit the powerful feature modeling capabilities of deep learning to estimate the spatial transformation between two images I_f and I_m. The overall structure of the proposed method is illustrated in Fig. 2. The proposed framework can be divided into two parts. The first part is based on the adaptive anatomical constraints and the second part is based on the cycle consistence constraints.

A. Adaptive Anatomy-Constraint

In this section, we introduce a medical image registration method based on the adaptive weak anatomical constraint. Medical image segmentation technology has developed rapidly in the past few years by using deep learning [19]–[21]. Segmentation of organs contains high-level information of the image and anatomical structures. Learning such high-level information assists the similarity based measures in training the model. However, direct use of binary label training network may lead to network overfitting [22]. Hu et al. [23] proposed to use a Gaussian filter to smooth labels, and then use multi-scale dice to calculate the similarity of labels. However, each pair of images is filtered by the same fixed filter, which may lead to over smoothed registration.

Inspired by their work, in this paper, we propose an adaptive anatomy-based registration method, where spatially smoothed probability mapping is performed on the label by using a Gaussian filter of the same size of the bounding box of the segmentation label. Let m_{gt} and f_{gt} indicate the anatomical label of moving image and fixed image, respectively. The mapping results are represented as $G_{l_m}(m_{gt})$, $G_{l_f}(f_{gt})$ respectively. $G()$ is a Gaussian filter, l_m, l_f respectively represent the size of the Gaussian matrix. Given a pair of training images, the registration network calculates a deformation field Φ to represent the correspondence: We use normalized cross correlation (NCC) to calculate the similarity between the smoothed labels as

$$L_{anatomy} = 1 - \mathrm{NCC}(T(G_{l_m}(m_{gt})), G_{l_f}(f_{gt})). \quad (2)$$

Fig. 3 shows the proposed adaptive anatomy-constrained image registration approach, which is a key component of our framework. As shown in the gray shadowed box in Fig. 2, the anatomical constraints based registration is applied to aligning $A \rightarrow B$ and $B \rightarrow A$, which produces the targeted registration result, and A and B respectively represent the image pairs to be registered. The output of this part is then input to the cycle constraint registration module, as shown in the light blue box in Fig. 2. There, the main purpose is to correct the displacement vector field generated by the adaptive anatomical constraint. For each part, the registration network g_ϑ aims to find a deformation field Φ that warps the I_m to I_f, so that the corresponding structures of the two images are aligned through the deformation field of

$$\Phi = g_\vartheta(I_f, I_m), \quad (3)$$

where ϑ denotes the learnable parameters of the registration network g.

It is worth noting that the segmentation labels in Fig. 3 are used only in the training phase to compute the network losses. In the testing stage, the proposed method generates a deformation field with only the input image pair and does not require label information.

B. Multi-task Network

The existing image registration algorithms based on deep learning are mostly unidirectional, ignoring the inherent inverse consistency of the transformation between image pairs [14], [15], [18]. Recently, Kim [24] proposed a cycle-consistent CNN registration network to study this aspect. However, different registration networks are used in this paper, and experimental parameters are added. The warped image is used as the fixed image, which increases the experimental error. At the same time, the article ignores the relationship between various processes. As shown in Fig.2, we propose a multi-task comprehensive registration network to exploit the inter-dependency among the tasks [25]. For images A and B, we have designed four different tasks, the first two tasks are that images A and B are symmetrically registered with each other, that is, use A as the moving image B as the fixed image: $G_{AB} : (A, B) \rightarrow \Phi_{AB} \rightarrow \bar{A}$ and Symmetrical: $G_{BA} : (B, A) \rightarrow \Phi_{BA} \rightarrow \bar{B}$; Subsequently, the last two tasks are to use the result of the first two tasks as the moving image, and the original image as the fixed image for registration. That is, $G_{\bar{B}B} : (\bar{B}, B) \rightarrow \Phi_{\bar{B}B} \rightarrow \hat{\bar{B}}$ and $G_{\bar{A}A} : (\bar{A}, A) \xrightarrow{\wedge} \Phi_{\bar{A}A} \rightarrow A$; where Φ_{AB} (resp. Φ_{BA}, $\Phi_{\bar{B}B}$, $\Phi_{\bar{A}A}$) denotes the deformation field from A to B (resp. B to A, $\bar{B}$ to B, $\bar{A}$ to A), $\bar{A}$, $\bar{B}$, $\hat{\bar{A}}$ and $\hat{\bar{B}}$ respectively indicate the registration result. Due to the large deformation of the initial images G_{AB} and G_{BA}, Conversely, for tasks

International Journal of Scientific Research in Engineering and Management (IJSREM)
Volume: 06 Issue: 05 | May - 2022 Impact Factor: 7.185 ISSN: 2582-3930

$G_{\bar{A}A}$ and $G_{\bar{B}B}$, the deformed image is then registered with the original image as a fixed image, and the task becomes simple, so we use cycle consistency loss for training. At the same time, the four tasks promote each other, and the later chapters will introduce them in detail. In general, the moving image is deformed using the deformation field estimated by the registration network, thereby training the registration network to minimize the difference between the deformed moving image and the fixed image. It is worth noting that the four tasks are completed through the same registration network and the weights are shared.

C. Inverse Constraint

At present, the most deep learning based algorithm does not consider the inverse consistency of the image. Inspired by some classical registration algorithms, such as [26], [27], we propose an inverse consistency constraint that encourages the transformation between pairs of images to be reversible. In our work, registering image A to B is opposite to registering image B to A. Thus, the obtained deformation field should be reciprocal. However, calculating the inverse of the deformation field is a cumbersome process, which may result in large error [27]–[29]. So we use the method shown in Fig.4 to ensure that the deformation field is reversible. $A \rightarrow B$ and $B \rightarrow A$ are reciprocal process, while $A \rightarrow B$ and $\bar{A} \rightarrow A$ also are reciprocal process, so $B \rightarrow A$ and $\bar{A} \rightarrow A$ are the same process, that is, the deformation field $\Phi_{AB} = \Phi_{\bar{B}B}$, the same also has Φ_{BA} and $\Phi_{\bar{A}A}$. Therefore, the proposed inverse consistency constraint is defined as

$$L_{inverse} = ||\Phi_{AB} - \Phi_{\bar{B}B}||_1 + ||\Phi_{BA} - \Phi_{\bar{A}A}||_1, \quad (4)$$

where $||\cdot||$ denotes L1 norm regularization. Here, we would like to minimize the difference between Φ_{AB} and $\Phi_{\bar{B}B}$ as well as between Φ_{BA} and $\Phi_{\bar{A}A}$. In this way, we ensure the reversibility of the deformation field and make the four tasks related to each other. By this method, the inverse consistency property of the transformation to be estimated can be explicitly modeled in the registration network. In this way, the complicated calculation and error caused by estimating the inverse deformation field are avoided, and the registration accuracy is further improved.

D. Cycle Constraint

The problem of many image registration techniques is that the correspondence between two images cannot be determined uniquely. In general, the cost function has many local minima due to the complexity of image registration. It is these local minima that cause the estimated transformation from image A to B to be different from the inverse of the estimated transformation from B to A [27].

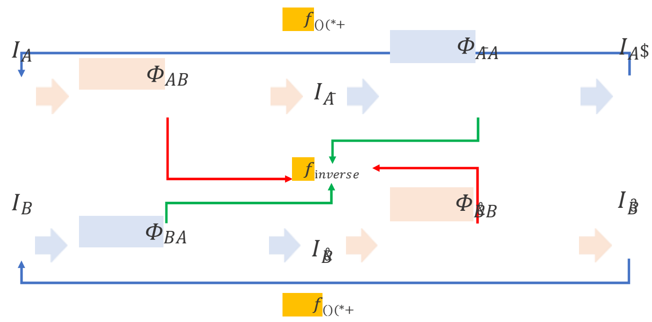

Fig. 4: The overall framework and task relationship diagram of the proposed multi-task registration network. $\Phi_{AB}, \Phi_{BA}, \Phi_{\bar{A}A}, \Phi_{\bar{B}B}$ respectively represent the deformation field generated by different tasks.

image B to image A, there is also $B \triangleq B$. We enforce this behavior using a cycle constraint

$$L^{cycle} = ||A - \hat{A}||_1 + ||B - \hat{B}||_1. \quad (5)$$

In this way, the reversibility of the image after deformation is improved, so that the deformation field is more in line with the physical deformation.

E. Deformation Field Constraint

In the process of image registration, proper constraint on deformation field is the key to the success of image registration. Appropriate constraints not only reduce the incorrect registration, but also make the deformation of the image more in line with the physical meaning. In this paper, the deformation field is constrained from three aspects, namely smoothness, anti-folding and range constraint:

$$L_{deform} = \alpha L_{smooth} + \beta L_{ant} + \gamma L_{ran} \quad (6)$$

where α , β and γ are positive weighting parameters which are used to balance the contributions of the smoothness, anti-folding and range constraint respectively.

1) Smoothness Constraint: Image registration algorithms typically use regularization techniques to achieve spatial smoothing and physically trusted spatial transformation. In previous studies, the deformation field to be estimated is generally smoothed by the smoothness constraint of its spatial gradient [18], [30]. We also use the same regularization to smooth the deformation field:

$$L_{smooth} = \sum_{p\in\Omega} ||\nabla\Phi(p)||^2, \quad (7)$$

where $\nabla\Phi(p)$ is the gradient of Φ at the pixel p, $||\cdot||$ represents the l_2 norm. Here, we use the difference between adjacent pixels to approximate the spatial gradient.

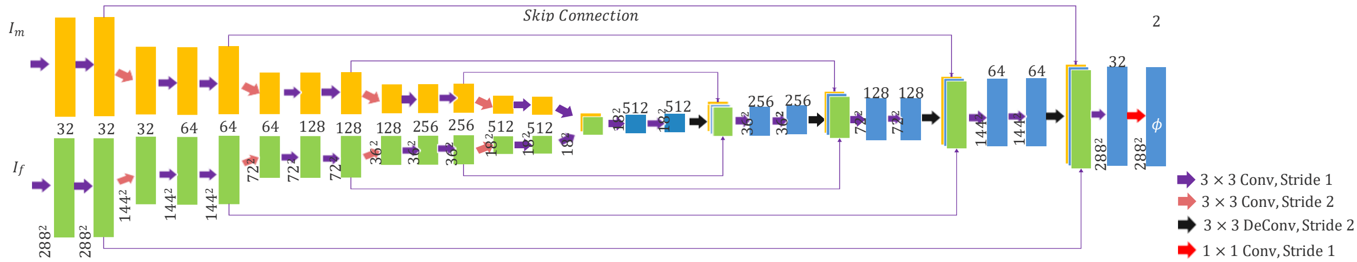

Fig. 5: Structure of the proposed registration network g.

When the weight of smoothness constraint is large, the registration precision decreases. When the weight of smoothness constraint is small, the image deformation is usually large, resulting in more folds. So how to choose the right weight is a challenging question. In this section, we will introduce an anti-folding constraint [31] to reduce folds:

$$L_{ant} = \sum_{p\in\Omega} Relu(-(\nabla\Phi(p)+1))\|\nabla\Phi(p)\|^2 \tag{8}$$

$Relu$ is used to penalize the gradient of the deformation field at the locations with foldings. That is, $\nabla\Phi(p)+1 \leq 0$, $Relu(-(\nabla\Phi(p)+1)) = -(\nabla\Phi(p)+1)$, otherwise, $Relu(-(\nabla\Phi(p)+1)) = 0$. That is to say, when a point p is folded on the x-axis or the y-axis, we penalty the gradient of this position and make its gradient smaller. Conversely, when $\nabla\Phi(p)+1 > 0$, it means there is no folding, we don't penalty the gradient here.

2) Range Constraint: In the previous chapters, we have discussed the smoothness and anti-folding of the deformation field. Although the smoothing constraint makes the image after registration more smooth, the anti-folding restriction reduces the folding of the deformation field, it cannot avoid that the pixel point after the displacement in the registration process exceeds the range of the image, the classical method is to exceed the scope of the pixel truncated, inevitably cause the wrong registration. In order to solve this problem, we propose a deformation field range constraint as:

$$L_{ran} = \sum_{p\in\Omega} f(h(\Phi(p)))\|\nabla\Phi(p)\|^2 \tag{9}$$

Where $h(\Phi(p))$ represents the displacement of the sampling grid.$f()$ is a piecewise function,

$$f(h(\Phi(p))) = \begin{cases} 0, & 0 < h(\Phi(p)) < S \\ |h(\Phi(p))|, & otherwise \end{cases} \tag{10}$$

where S indicates the size of the image.

F. Network Architecture and Implementation

To achieve multi-task learning with the same network, we design a multi-scale fusion network structure, which uses two paths to learn the feature information of fixed image and moving image respectively, I_m which is the classic registration network. We use two different convolution neural network respectively to extract the feature of I_f and I_m, and then the feature map is multi-scale fused to predict the deformation field. In this way, both the unique feature information of the moving image and the fixed image are learned, and the common feature information is also learned. Refer to Unet [32] using skip connection to propagate features learned in the encoding phase directly to the decoding layer makes the output deformation field more accurate. Input image pair A, B, by changing the input path of image A, B, both image A can be registered to image B and image B can be registered to image A. that is, the forward transformation and the reverse transformation of images can be obtained respectively. ReLU activation and batch normalization are applied in every layer. Convolution kernel size is 3×3, if not explicitly noted. We also use convolution stride size of 2 instead of the pooling layer to retain more information. In the last layer, we use a 1×1 convolutional layer to reduce the number of feature maps to obtain deformation field.

Accordingly, the loss function of our proposed approach for deformable registration is formulated as

$$L = w_0 L_{anatomy} + w_1 L_{cycle} + w_2 L_{inverse} + w_3 L_{deform} \tag{11}$$

where w_0, w_1, w_2, w_3 are positive weighting parameters. In the above equation, $L_{anatomy}$ represents the adaptive anatomical loss and is used to implement task G_{AB} and G_{BA}. L_{cycle} represents the cycle constraint loss and is used to implement task $G_{\bar{B}B}$ and $G_{\bar{A}A}$. $L_{inverse}$ is the inverse constraint loss. Because these four tasks are equal, we chose the same weight so that the four tasks can be effectively registered. L_{deform} represents the regularization loss of the deformation field includes three parts, and the optimal weight is selected through experiments.

The registration network g is trained by optimizing the loss function in (11) using the training data. The input of the registration network is I_m and I_f, and the output is the deformation field Φ based on a set of parameters ϑ, the kernels of the convolutional layers. Our proposed method was implemented based on Tensorflow [33],

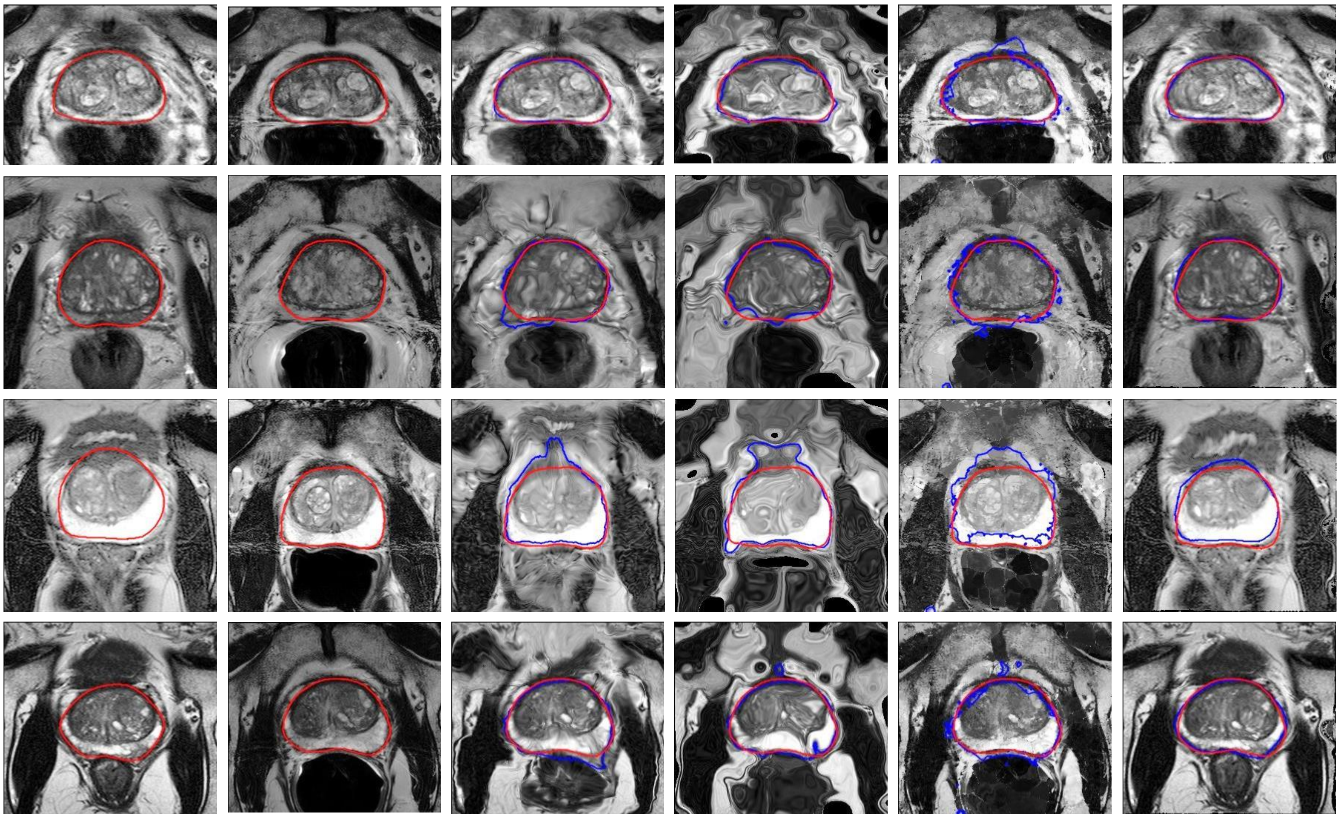

Fig. 6: Example MRI slices of input and output by different methods. Red contours denote the prostate boundary of I_m and I_f, blue contours denote the prostate boundary after registration.

III. EXPERIMENTS

A. Materials and Evaluation

In order to verify the effectiveness of our proposed method, we collected prostate MR images from 70 subjects. For each subject, the data include two prostate MR images acquired more than one year apart, one with and the other without using ERC. Before the experiment, we preprocessed the collected data. First, since the ranges of image pixel intensity values of different images vary significantly, we calculated the average pixel intensity of all subjects and used a histogram matching algorithm [34] to map the images into the same range. Second, the resolutions of prostate MR images collected at different times can be very different, where the voxel sizes are 0.2734mm × 0.2734mm × 3.0mm and 0.3516mm × 0.3516mm × 3.0mm for images with and without ERC, respectively. Thus, we resampled the images to the same resolution of 0.2734mm × 0.2734mm × 3.0mm to reduce the potential loss of image information. We performed a five-fold cross-validation to evaluate the performance of the proposed method. In each fold, the training set consists of 56 subjects and the test set has 14 subjects.

Since there is no ground truth deformation field available, we measure the registration performance indirectly via the provided prostate segmentation masks which were annotated by radiologists. Dice sore and Hausdorff distance (HD) can intuitively observe the alignment accuracy of prostate anatomical structure. Dice score and Hausdorff distance (HD) are computed by prostate masks of fixed and warped moving images. A dice score of 1 indicates the same structure, and a score of 0 indicates no overlap. Hausdorff distance is used to measure the accuracy of prostate margin alignment, and usually the smaller the value, the better the result. Furthermore, to quantify the degree of deformation regularity, we calculate the percentage of the non-positive Jacobian determinant, i.e. Det-Jac<0, of the deformation field. Smaller percentage indicates smoother deformation field. The following sections will analyze the experimental results in detail.

B. Comparison with Other Methods

In order to better measure the performance of our proposed method, we compared it with the classical method based on iterative optimization and the method based on deep learning.

International Journal of Scientific Research in Engineering and Management (IJSREM)
Volume: 06 Issue: 05 | May - 2022 Impact Factor: 7.185 ISSN: 2582-3930

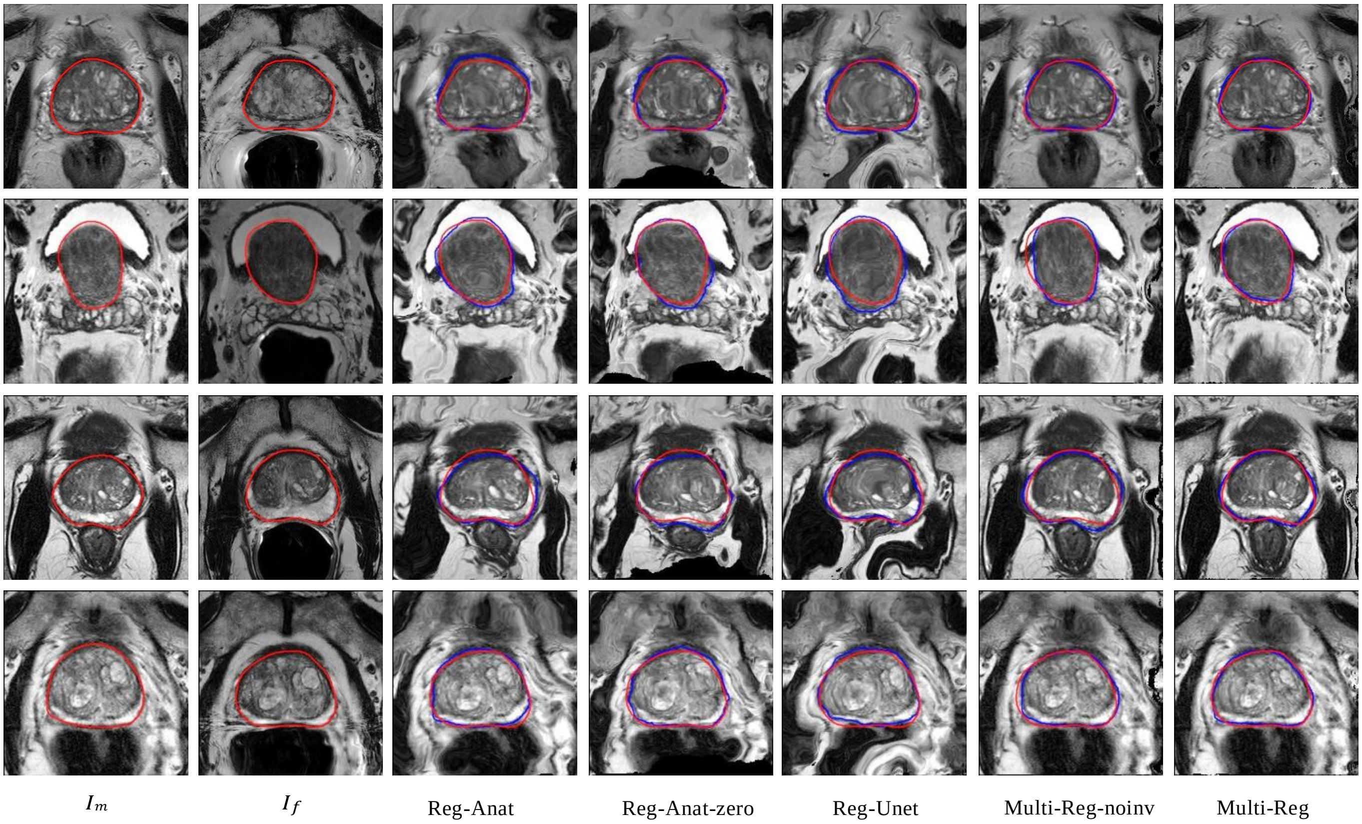

Fig. 7: Example MRI slices of registration results with overlayed segmentation contours obtained in the ablation studies.

TABLE I: Performance comparison of different methods.

Method	Dice (%)	HD (mm)	Det-Jac<0 (%)
Initialization	82.55 ±0.02	98.66 ±0.63	–
SyN [35]	93.19 ±0.01	9.03 ±0.55	–
DIRNet [14]	90.28 ±0.01	15.39 ±0.39	4.54 ±0.01
Voxelmorph	89.54 ±0.01	29.22±8.56	5.77±0.01
Multi-Reg (ours)	**89.36 ±0.01**	**8.39 ±0.60**	**0.85±0.01**

Firstly, we compared our approach to Symmetric Normalization (SyN) [35] that is known to have its state-of-the-art performance among the classical approaches, this method can maximize the cross-correlation within the space of diffeomorphic maps. We perform a wide parameter search to select the best experimental results as a comparison method. Usually, the experimental results of this method are as good as those of the deep learning-based method. Next, we compared our approach with two other deep learning based algorithms, including DIRNet [14] and VoxelMorph [30]. DIRNet optimizes registration based on similarity measures, while VoxelMorph directly estimates the transformation field.

The average Dice score and HD as well as the standard deviation between the warped moving image and fixed image are shown in Table I. The conventional algorithm SyN improves Dice score over the initialization, however, has even worse HD compared to the starting point. As shown in Fig 6, it can be seen that the matching of the edges of the prostate is not good. The DIRNet didn't perform well in either Dice or HD, because it couldn't handle the large deformation between MR images with and without ERC. The method of Voxelmorph also failed to register the large deformation between image pairs due to the use of simple similarity measurement as loss function for network training. Furthermore, as shown in Table I, the proposed method produces less non-positive Jacobian determinant of the deformation field, which is a very good indication of maintaining the topological structure of the images.

Some qualitative results of comparative method are shown in Fig 6. It can be seen that our proposed Multi-Reg produces accurate registration results, which have more overlap with the segmentation of fixed images. In addition, Multi-reg produces much smoother warped images. In terms of the running time, our proposed algorithm and other deep learning algorithms are able to register image pairs with less than a second, which is significantly faster than the traditional iterative registration.

C. Ablation Studies

To analyze the impact of our proposed method on the performance of registration, we compared the performance of the proposed Multi-Reg with different losses and structure.

Volume: 06 Issue: 05 | May - 2022 Impact Factor: 7.185 ISSN: 2582-3930

TABLE II: Performance evaluation through ablation studies.

Method	Dice (%)	HD (mm)	Det-Jac< 0 (%)
Initialization	82.55 ±0.02	98.66 ±0.63	–
SyN [35]	93.19 ±0.01	9.03 ±0.55	–
DIRNet [14]	90.28 ±0.01	15.39 ±0.39	4.54 ±0.01
Voxelmorph	89.54 ±0.01	29.22±8.56	5.77±0.01
Multi-Reg (ours)	**89.36 ±0.01**	**8.39 ±0.60**	**0.85±0.01**

the anatomical constraint $L_{anatomy}$ and deformation field constraint L_{deform} as the basic comparison method of ablation experiment (Reg-anat). In order to verify the influence of our proposed range constraints on the experimental results, the range constraint weights are adjusted to zero (Reg-Anat-zero). To demonstrate the effectiveness of our proposed registration network structure, we replaced the encoder of our registration network with a single path, which essentially becomes a Unet (Reg-Unet). Specifically, we maintain the same number of parameters in both networks. The above experiments are single-task experiments, that is, $G_{AB} : (A, B) \to \Phi_{AB} \to \bar{A}$. To measure the performance of multi-task registration network, we indicated the proposed multi-task registration network as Multi-Reg, including: $G_{AB} : (A, B) \to \Phi_{AB} \to \bar{A}$, $G_{BA} : (B, A) \to \Phi_{BA} \to B$, $G_{\bar{B}B} : (B, B) \to \Phi_{\bar{B}B} \to \hat{B}$ and $G_{\bar{A}A} : (\bar{A}, A) \xrightarrow{\wedge} \Phi_{\bar{A}A} \to A$. we also denoted the multi-task registration network without inverse constraints as Multi-Reg-noinv.

Table II shows the ablation study results. The performance difference between Reg-Anat and Reg-Unet shows the advantage of our proposed network structure of two paths with adaptive anatomical constraint. Comparing Reg-Anat and Reg-Anat-zero shows that the range of constraints has a slight improvement on the experimental results by regularizing the deformation field. It reduces the incorrect displacement of the point and the folding of the aligned image. For the multi-task registration network experiment, comparing Multi-Reg and Multi-Reg-noinv shows that adding inverse constraints can better achieve multi-tasking registration and improve the inverse consistency between image pairs. Some qualitative results of comparative method are shown in Fig. 7. It can be seen that the Multi-Reg proposed by us is more accurate in the registration of prostate edge and the image after registration is smoother.

D. Weight Analysis

Varying the weight of each constraint can change the experimental results. In order to evaluate the effects of the weights on registration of prostate MR images, we conducted a weight analysis experiment and selected the optimal weight. Since $L_{anatomy}$ is our main loss, we first set its weight w_0 to be 1 and then conducted an empirical search of the weight combinations on w_1, w_2 and w_3.

Fig. 8(a) shows the experimental results of varying the weight parameters w_1 and w_2. We can see that when $w_1 = 1$ and $w_2 = 1$,

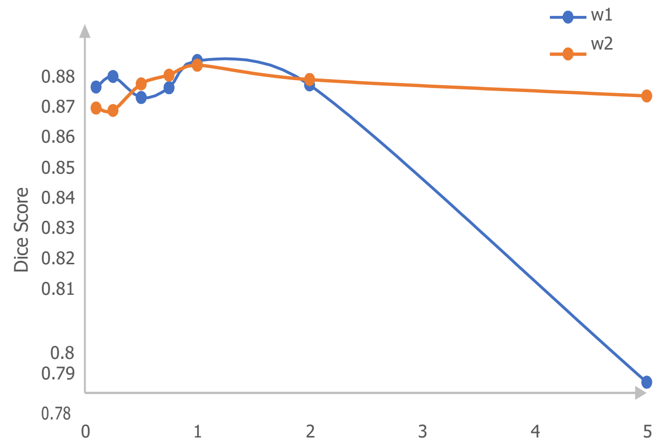

(a) Weight parameters w_1 and w_2

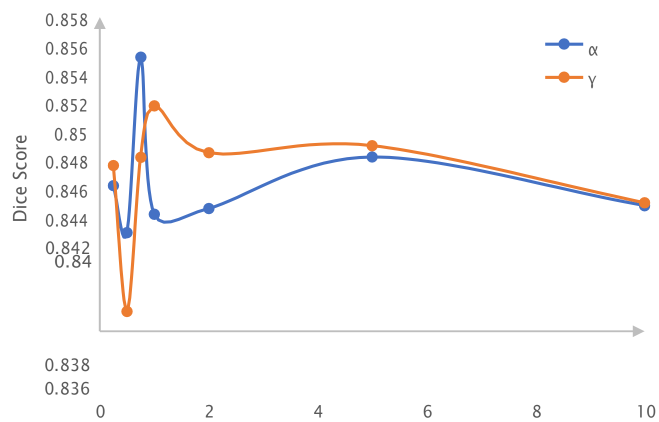

(b) Regularization parameter α and γ

Fig. 8: (a) Effects of varying the weight parameters w_1 and w_2 on Dice score. The best performance was achieved when $w_1 = 1$ and $w_2 = 1$; (b) Effects of varying the regularization parameter α and γ on Dice score. The best results occur when $\alpha = 0.75$ and $\gamma = 1.0$.

is used to implement tasks $A \to B$ and $B \to A$. The loss L_{cycle} is used to implement task $\bar{A} \to A$,$\bar{B} \to B$, and $L_{inverse}$ is used to constrain the reversibility of the deformation field.

For the regularization of the deformation field, since the four tasks all use the regularization of the deformation field, it is particularly important to select the appropriate deformation field regularization coefficient. Fig. 8(b) shows the effects of varying the regularization parameter α and γ, the two components of w_3, on Dice scores. This experiment also shows the importance of regularization on deformation field, as demonstrated by the results in Fig. 9. Choosing a suitable regularization weight is very important. If the weight is too large, it is overly encouraged, resulting in inaccurate registration results. If the weight is too small, it will cause unreasonable deformation. For the three regularization methods used in this paper, we performed a parametric analysis experiment.

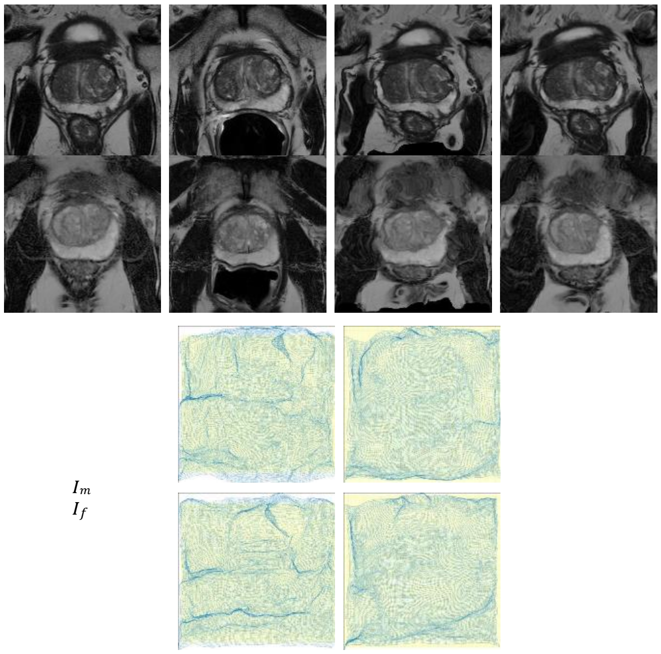

Reg-Anat-zero Reg-Anat

Fig. 9: Examples of using range constraints or not, below the image is the corresponding deformation field, where the yellow line is the initial grid and the blue line is the grid after the deformation. range constraint can make the deformation field predicted by the network smoother and thus restrain the image deformation beyond the range of the image. In addition, it helps prevent the black blocks in images caused by the modification of the deformation field by clipping, which makes the predicted deformation field more robust.

IV. Conclusions

In this paper, a multi-task registration network based on deep learning is proposed. This method can use the same network to achieve different registration tasks, make better use of image feature information. At the same time, the inverse constraint is used to improve the inverse consistency between image pairs and adaptive anatomical constraints make use of advanced characterization information to make the registration network more focused on the region of interest. In addition, we propose a range constraint to further normalize the deformation field so that the deformation of the image is more in line with the motion rules. It is worth noting that the proposed method can be trained in an end-to-end fashion. In the testing stage, the proposed method generates a deformation field with one single forward pass without iterative optimization and does not require label information. Therefore, once the training is completed, our model can quickly register images within one second. In addition, from the application point of view, this is the first work targeting at registering prostate MR images of the same subject acquired at different time points with and without ERC.

Although our method performed better on prostate MR images with and without ERC by achieving more realistic results when compared with other existing methods, our method also comes with limitations. First, due to the limitations of the data, where large interslice distance exists, our method was only evaluated on 2D images. The method can be extended for 3D registration when there is suitable dataset. Second, the proposed method was evaluated using only prostate boundary segmentation. In our future work, we will explore using internal landmarks, for example, prostate tumors, to further evaluate our method to make it more clinically meaningful.

References

[1] M. LaSpina and G. P. Haas, “Update on the diagnosis and management of prostate cancer,” *Can J Urol*, vol. 15, no. Suppl 1, pp. 3–13, 2008.
[2] E. M. Charles-Edwards and N. M. deSouza, “Diffusion-weighted magnetic resonance imaging and its application to cancer,” *Cancer imaging*, vol. 6, no. 1, p. 135, 2006.
[3] J. P. Pluim, J. A. Maintz, and M. A. Viergever, “Image registration by maximization of combined mutual information and gradient information,” in *International Conference on Medical Image Computing and Computer-Assisted Intervention*. Springer, 2000, pp. 452–461.
[4] D. Rueckert, M. J. Clarkson, D. L. Hill, and D. J. Hawkes, “Non-rigid registration using higher-order mutual information,” in *Medical Imaging*. SPIE, 2000, pp. 438–448.
[5] X. Cao, J. Yang, Y. Gao, Q. Wang, and D. Shen, “Region-adaptive deformable registration of CT/MRI pelvic images via learning-based image synthesis,” *IEEE Transactions on Image Processing*, vol. 27, no. 7, pp. 3500–3512, 2018.
[6] T. Vercauteren, X. Pennec, A. Perchant, and N. Ayache, “Diffeomorphic demons: Efficient non-parametric image registration,” *NeuroImage*, vol. 45, no. 1, pp. S61–S72, 2009.
[7] J. P. Pluim, J. A. Maintz, and M. A. Viergever, “Mutual-information-based registration of medical images: a survey,” *IEEE transactions on medical imaging*, vol. 22, no. 8, pp. 986–1004, 2003.
[8] F. Maes, A. Collignon, D. Vandermeulen, G. Marchal, and P. Suetens, “Multimodality image registration by maximization of mutual information,” *IEEE transactions on Medical Imaging*, vol. 16, no. 2, pp. 187–198, 1997.
[9] H. Luan, F. Qi, Z. Xue, L. Chen, and D. Shen, “Multimodality image registration by maximization of quantitative–qualitative measure of mutual information,” *Pattern Recognition*, vol. 41, no. 1, pp. 285–298, 2008.